ELSEVIER

Chemical Engineering Journal 79 (2000) 187–195

Chemical Engineering Journal

www.elsevier.com/locate/cej

Electrochemical removal of nickel ions from industrial wastewater

K.N. Njau, M. vd. Woude, G.J. Visser, L.J.J. Janssen*

Department of Chemical Engineering, Laboratory of Process Development, Eindhoven University of Technology, P.O. Box 513, 5600 MB Eindhoven, The Netherlands

Received 4 November 1998; accepted 18 June 1999

Abstract

The electrochemical reduction of nickel ions in dilute industrial wastewater from a galvanic nickel plating plant was carried out on a three-dimensional electrode in a gas diffusion electrode packed bed electrode cell (GBC) and also on a rotating disc electrode. To explain the experimental results, concentration profiles for selected species were calculated during nickel deposition.

It was found that, depending on the solution composition and electrolysis conditions, metallic nickel, nickel oxide and nickel hydroxide, as well as nickel oxyhydroxide, can be deposited. Metallic nickel dendrite formation and its growth towards and on the Nafion membrane were identified as a major problem in a cell with a small interelectrode gap due to the damage caused on the gas diffusion electrode (GDE) membrane assembly. Moreover, it was found that the nickel selectivity ratio depends on the total current density as well as on the Ni^{2+} concentration, and that the surface of the rotating disc electrode can be completely blocked by green nickel hydroxide deposit.

Keywords: Electrochemical removal; Nickel ions; Industrial wastewater

1. Introduction

Electrochemical recovery of nickel from rinse water is of interest because pure metal may be recovered for recycling in one stage without the necessity of sludge disposal and regeneration of saturated ion exchanger resin. Problems with the electrochemical treatment of rinse water from the plating industry are the low concentration of the electroactive species and the low conductivity due to a lack of supporting electrolyte and a relatively high pH.

The use of designs with high surface area electrodes or enhanced mass transfer improves the process. The current needed for the removal of metal ions is low and, because the energy consumption is not critical, low current efficiencies may be acceptable. A major drawback of a three-dimensional electrode in a poor conducting solution is the excessive ohmic potential drop in the solution, so that the electrode reaction penetrates the electrode matrix poorly. This condition becomes more critical for solutions with a very little supporting electrolyte. Operation with a three-dimensional electrode requires the careful selection of the electrolytic conditions.

The use of a gas diffusion electrode packed bed electrode cell (GBC) reactor for the reduction of metal ions has been extensively covered in [1–5]. The reduction of nickel using model solutions was investigated earlier, first with a rotating disc electrode (RDE) system [1] and later in a GBC reactor [2].

In this work, the behaviour of a GBC reactor in an industrial solution has been investigated using a pilot GBC plant, and the concentration profiles of selected species in the diffusion layer have been calculated using experimental results obtained with an RDE system. Experiments have also been carried out in a laboratory scale GBC reactor using the same industrial solution. The effects of the electrolysis current density, nickel ion concentration, UV treatment, the nature of the deposit obtained and the deposit penetration depth into the three-dimensional cathode are reported.

2. Theory

The interpretation of what is happening during nickel deposition from a dilute buffered solution can be best understood from a simulation of the concentration profiles at the cathode. The concentration profiles during nickel deposition from dilute buffered solutions are modelled using the approach presented in [5–8]. Let us consider a nickel sulphate bath with boric acid as a buffering agent being used to deposit nickel on an RDE. The material balance equation

* Corresponding author. Tel.: +31-40-2473591; fax: +31-40-2453762.
E-mail address: d.c.m.tjallema-dekker@tue.nl (L.J.J. Janssen).

1385-8947/00/$ – see front matter
PII: S1385-8947(00)00210-2

Nomenclature

A_g	geometric surface area (m^2)
$C_{j,s}$	concentration of species j on the electrode surface ($mol\,m^{-3}$)
D_j	diffusion coefficient for species j ($m^2\,s^{-1}$)
F	Faraday's constant (96 487 C)
i	current density ($A\,m^{-2}$); $i=I/A_g$
i_H	hydrogen current density ($A\,m^{-2}$)
i_{Ni}	nickel current density ($A\,m^{-2}$)
i_T	total current density ($A\,m^{-2}$)
I	current (A)
K_i	equilibrium constant for reaction i
K_{sp}	solubility product
N_j	molar flux of species j ($mol\,m^{-2}\,s^{-1}$)
Q_{Ni}	charge used for nickel deposition (C)
Q_T	total charge used during nickel deposition (C)
R	gas constant ($8.3143\,J\,mol^{-1}\,K^{-1}$)
R_j	production rate of species due to homogeneous reactions ($mol\,m^{-3}\,s^{-1}$)
S_{Ni}	nickel selectivity ratio $S_{Ni}=i_{Ni}/i_H$
t	time (s)
T	temperature (K)
x	distance in the normal direction to the electrode surface (m)
z_j	charge on species j

Greek symbols

δ_N	thickness of the Nernst diffusion layer (m)
ν	fluid kinematic viscosity ($m^2\,s^{-1}$)
ω	disc rotational speed ($rad\,s^{-1}$)

for species j can be written as

$$\frac{\partial C_j}{\partial t} = -\nabla \cdot N_j + R_j \tag{1}$$

In this solution, the following homogeneous reactions are considered to be fast and therefore in equilibrium

$$Ni^{2+} + OH^- = NiOH^+ \tag{a}$$

$$H_2O = H^+ + OH^- \tag{b}$$

$$HSO_4{}^- = H^+ + SO_4{}^{2-} \tag{c}$$

$$H_3BO_3 = H^+ + H_2BO_3{}^- \tag{d}$$

$$Ni^{2+} + 2H_2BO_3{}^- = Ni(H_2BO_3)_2 \tag{e}$$

The mono-complex formation between Ni^{2+} and $H_2BO_3{}^-$ ions can be neglected at high ionic strength of the medium [9]. It is assumed that this is also the case for the solution used in this study.

Equations relating the concentrations of the species can be drawn from these equilibria and dissociation constants. The problem is considered as one-dimensional, where the mass transport is determined by diffusion only. This is a simplification as there is also a small contribution to the mass transfer by migration.

Neglecting migration, the transport equation for each species can be formulated by

$$D_j \frac{d^2 C_j}{dx^2} = -R_j \tag{2}$$

In addition to transport equations, the species must satisfy the electroneutrality condition everywhere in the system, i.e.

$$\sum_{j=1}^{NS} z_j C_j = 0 \tag{3}$$

At steady state, mass balance equations for the different species are written as follows

$$R_{Ni} + R_{NiOH} = 0 \tag{4}$$

$$R_{HSO_4} + R_{SO_4} = 0 \tag{5}$$

$$R_H + R_{HSO_4} - R_{NiOH} - R_{OH} + R_{H_3BO_3} - R_{H_2BO_3} - 2R_{Ni(H_2BO_3)_2} = 0 \tag{6}$$

$$R_{H_3BO_3} + R_{H_2BO_3} + 2R_{Ni(H_2BO_3)_2} = 0 \tag{7}$$

These equations together with the electroneutrality equation and the equilibrium equations which can be derived from reactions (a)–(e) constitute the set of expressions to be solved throughout the diffusion layer. The flux of each species is obtained by integrating Eqs. (4)–(7).

The following electrode reactions occur on the cathode surface

$$Ni^{2+} + 2e^- = Ni \tag{f}$$

$$2H_2O + 2e^- = H_2 + 2OH^- \tag{g}$$

The boundary conditions at the electrode surface (x=0) account for the fact that the total current for a particular component must match the net flux of all species containing the component and are given by

$$\frac{i_{Ni}}{2F} = -D_{Ni}\frac{dC_{Ni}}{dx} - D_{NiOH}\frac{dC_{NiOH}}{dx} - D_{Ni(H_2BO_3)_2}\frac{dC_{Ni(H_2BO_3)_2}}{dx} \tag{8}$$

$$\frac{i_H}{F} = -D_H\frac{dC_H}{dx} + D_{NiOH}\frac{dC_{NiOH}}{dx} + D_{Ni(H_2BO_3)_2}\frac{dC_{Ni(H_2BO_3)_2}}{dx} + D_{OH}\frac{dC_{OH}}{dx} - D_{HSO_4}\frac{dC_{HSO_4}}{dx} - D_{H_3BO_3}\frac{dC_{H_3BO_3}}{dx} \tag{9}$$

It is also assumed that the total concentration for the sulphate and borate species remains constant

$$C_1 = C_{HSO_4} + C_{SO_4} \tag{10}$$

Table 1
Calculation parameters

Parameter	Value	Dimensions	Ref.
D_{H^+}	9.30×10^{-9}	($m^2\ s^{-1}$)	[7]
D_{NiOH^+}	1.00×10^{-9}	($m^2\ s^{-1}$)	[7]
D_{OH^-}	5.26×10^{-9}	($m^2\ s^{-1}$)	[5]
$D_{HSO_4^-}$	1.33×10^{-9}	($m^2\ s^{-1}$)	[10]
$D_{SO_4^{2-}}$	1.07×10^{-9}	($m^2\ s^{-1}$)	[10]
$D_{NiH_2BO_3^+}$	1.00×10^{-9}	($m^2\ s^{-1}$)	Assumed
$D_{H_3BO_3}$	1.53×10^{-9}	($m^2\ s^{-1}$)	[11]
$D_{H_2BO_3^-}$	1.53×10^{-9}	($m^2\ s^{-1}$)	[11]
D_{Ni^+}	5.64×10^{-10}	($m^2\ s^{-1}$)	[6]
K_a	$1.26\times10^{+1}$	($mol^{-1}\ m^3$)	[12]
K_b	1.00×10^{-8}	($mol^2\ m^{-6}$)	[13]
K_c	$1.30\times10^{+1}$	($mol\ m^{-3}$)	[13]
K_d	6.3×10^{-7}	($mol\ m^{-3}$)	[9]
K_e	8.10×10^{-2}	($mol^{-2}\ m^6$)	[9]
$K_{sp,Ni(OH)_2}$	6.3×10^{-7}	($mol^3\ m^{-9}$)	[12]
$\delta_{N,Ni}$	1.023×10^{-5}	(m)	Calculated

$$C_2 = C_{H_2BO_3} + C_{H_3BO_3} + 2C_{Ni(H_2BO_3)_2} \quad (11)$$

The Nernst diffusion layer thickness δ_N on a RDE for a species j is given by

$$\delta_{N,j} = 1.62\left(\frac{3D_j}{\nu}\right)^{1/3}\left(\frac{\omega}{\nu}\right)^{-1/2} \quad (12)$$

Introducing the relations for the equilibrium constants for reactions (a)–(e) into Eqs. (8) and (9) for a bulk solution with a fixed composition, the partial current densities can then be expressed in terms of two variables, namely C_{Ni} and C_H. This provides two linear differential equations. The same treatment as proposed in [7] is used, whereby the equations obtained are rewritten in a matrix form. A computer program was developed which utilizes FORTRAN routines to solve a system of linear differential equations.

Table 1 shows the values of the constants at 293 K supplied to the program to solve the equations. Moreover, the diffusion layer thickness of the Ni^{2+} species at a rotation rate of 25 rev s^{-1} was used as a boundary condition and the precipitation of $Ni(OH)_2$ was taken into account.

The experimental partial current densities at selected current densities for a graphite RDE with a rotating speed of 25 rev s^{-1} in the spare tank solution containing 40 mol m^{-3} Ni^{2+} ions were used to calculate the concentration profiles.

3. Experimental details

3.1. The nickel–chromium plating plant

The plant selected for this study has a typical nickel–chromium plating line with 28 open baths. Each bath is filled with 6 m^3 of solution. The process involves surface preparation, washing, plating and rinsing. The nickel plating bath is an $NiSO_4$–$NiCl_2$ solution buffered by boric acid. During operation, the concentration of Ni^{2+} in the first rinse tank, also known as the spare tank, rises gradually and reaches a maximum value of about 40 mol m^{-3} in 15 days of operation from the day of refreshing the spare tank. The compositions of the bath and the spare tank are given in Table 2.

Table 2
Concentration of selected species in the plating bath and the spare tank solution with the highest nickel concentration

Species	Concentration of species C_j (mol m^{-3})	
	Plating bath	Spare tank
Ni^{2+}	971	40
SO_4^{2-}	725	30
Cl^-	493	20
H_3BO_3	623	26

During nickel plating, four different solutions with organic additives are added to the bath. These additives are only known by their tradenames, namely, H(R) Glanztrager, Netzmittel DL, O2 Annzusatz Elpelyt SF/PP(R) and Glanztrager X5 (LPW Chemie). A mixture of these additives is added to the bath in the volume ratio H(R):DL:SF/PP(R):X5 of 5:5:9:5. For a bath volume of 6 m^3, about 0.1 m^3 of additive mixture is added. The four solutions with organic additives were analysed by mass spectroscopy. Only X5 could be clearly identified as being saccharin.

The nickel plated parts are rinsed in a series of washing units with a counter-current flow of rinse water, before being transferred further to the chrome plating section. Operation of the plant is continuous for 5 days in a week. At weekends, the process is partially shut down leaving the bath heaters and rinse water operating.

3.2. The RDE

Deposition of nickel from the spare tank solutions was investigated using a three-electrode cell system with a graphite RDE of 0.50 cm^2 geometric surface area, a platinum foil counter-electrode of 4 cm^2 surface area and a saturated calomel reference electrode with a Luggin capillary. The surface of the working electrode was mechanically polished and degreased before each experiment. Nickel solutions with various nickel sulphate concentrations between 5 and 40 mM were used. Lower concentrations than 40 mM were obtained by diluting the spare tank solution. The pH was adjusted by addition of a sodium hydroxide or a sulphuric acid solution and the temperature was kept at 293 K. Potentiostatic and galvanostatic experiments were conducted using an automatic data acquisition system (Autolab PGSTAT20 version 3.0, Eco Chemie B.V.). All potentials were measured with reference to the saturated calomel electrode without corrections for the solution ohmic drop.

Experiments to determine the selectivity ratio for nickel deposition were performed by galvanostatically depositing nickel, and thereafter coulometrically dissolving the Ni metal deposit anodically in a bath consisting of 0.1 M H_2SO_4 and 1.0 M NaCl to prevent passivation of nickel.

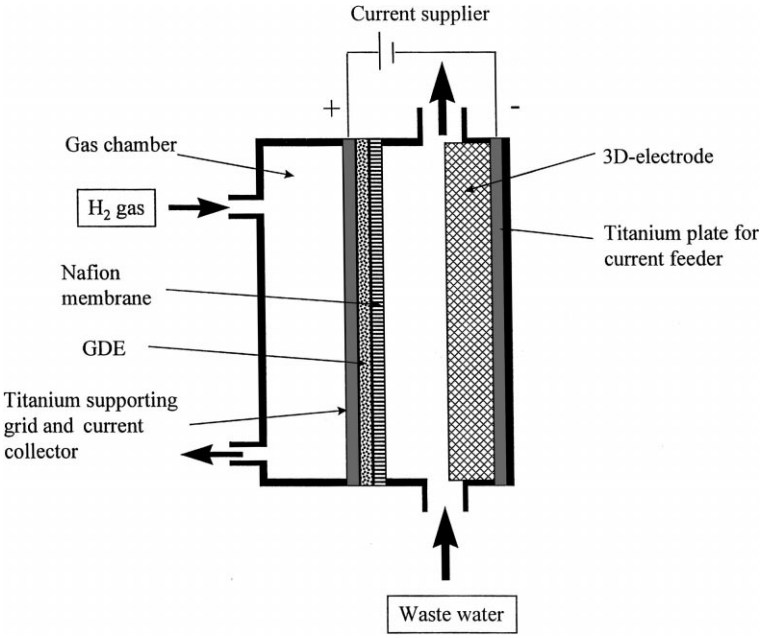

Fig. 1. Schematic representation of the GBC cell for nickel deposition.

The effects of the current density, UV treatment, nickel ion concentration and concentration of organic additives on the selectivity ratio for nickel deposition were experimentally determined. UV treatment was applied, as it is well known that some organic additives forming complexes with Ni^{2+} ions can be destroyed by UV irradiation.

3.3. The pilot plant

The pilot plant set-up was essentially a single-pass flow-by system consisting of two cells, a pump and a filter. The set-up was equipped with an UV lamp with a wavelength range from 190 to 400 nm (Berson HFS E 0.4). The solution flow rate was monitored through a flow meter. Moreover, a pH meter and a conductivity meter were installed on-line. A schematic representation of the GBC reactor is shown in Fig. 1. The anode was a gas diffusion electrode (GDE): a $4\times20\,cm^2$ fuel cell grade E-TEK solid polymer electrolyte electrode (ELAT) modified by pressing Nafion 117 membrane on the solution side. This modification was carried out by the ECN Company (Putten, The Netherlands). The cathode chamber had a thickness of 1 cm, a height of 20 cm and a width of 4 cm. The standard cathode consisted of a stack of 5–7 expanded nickel gauzes supported on a titanium back plate placed on the backside of the cathode chamber. The cathode filled only partially the cathode compartment. The pilot plant was installed to treat the nickel spare tank solution. A solution flow rate of $30\,cm^3\,s^{-1}$ through the pilot plant cell was used. Due to the large volume of the spare tank compared to the size of the pilot plant cell, the concentration in the spare tank solution was considered to remain constant.

4. Results

4.1. Nickel deposition on the RDE

4.1.1. Effect of current density on the selectivity ratio for nickel deposition

The current density was varied between 8 and $500\,A\,m^{-2}$. The solutions were the spare tank solution with an Ni^{2+} concentration of $40\,mol\,m^{-3}$ and a dilute solution with an Ni^{2+} concentration of $5\,mol\,m^{-3}$. The temperature of the experiment was maintained at 293 K. The charge used during nickel deposition Q_T and that for nickel dissolution Q_{Ni} were employed to calculate the partial current densities and the nickel selectivity ratio S_{Ni}, where

$$i_{Ni} = \frac{Q_{Ni}}{Q_T} i_T \tag{13}$$

$$i_H = \left(1 - \frac{Q_{Ni}}{Q_T}\right) i_T \tag{14}$$

$$S_{Ni} = \frac{i_{Ni}}{i_H} = \left(\frac{Q_{Ni}}{Q_T - Q_{Ni}}\right) \tag{15}$$

The effect of the current density on the nickel selectivity ratio S_{Ni} is shown in Fig. 2. From Fig. 2 it is seen that, for the solution with $40\,mol\,m^{-3}$ Ni^{2+} ions, $\log S_{Ni}$ increases steadily and linearly with increasing $\log i$ to about 20 at i=$250\,A\,m^{-2}$, and thereafter drops sharply with increasing $\log i$. At current densities higher than $250\,A\,m^{-2}$, the current efficiency for nickel deposition was very irregular, sometimes in line with the declining curve in Fig. 2 and in other cases practically zero, where greenish nickel hydroxide deposit was formed. For the 5 mM Ni^{2+} spare tank solution,

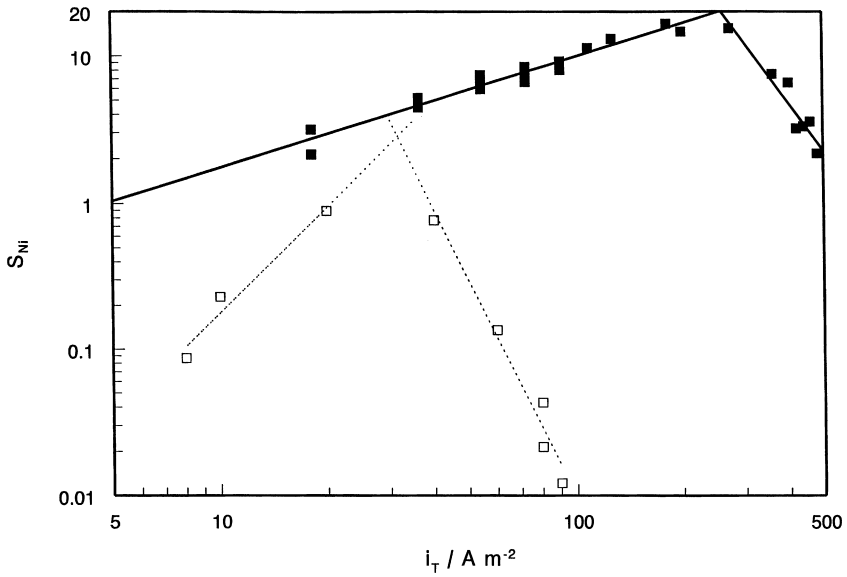

Fig. 2. Nickel selectivity ratio as a function of the total current density at 5 mol m^{-3} (□) and 40 mol m^{-3} (■) nickel ions. The pH values of the solutions were 6.9 and 6.3, respectively.

a similar result was obtained, but the slopes of the curves were much steeper.

The current densities $i_{Ni,\,max}$ for Ni deposition at the maxima of the log S_{Ni}/log i_T curves in Fig. 2 were 23 and 238 A m^{-2} for nickel concentrations of 5 and 40 mol m^{-3}, respectively.

Taking into account the ratio between the sulphate and chloride concentration and using $\delta_{N,\,Ni}$ from Table 1, it was calculated that the migration–diffusion limiting current densities $i_{Ni,\,g}$ for Ni deposition are equal to 120 and 959 A m^{-2} for Ni concentrations of 5 and 40 mol m^{-3}, respectively. The effect of the presence of boric acid was not considered, as boric acid at pH 6.32 is practically undissociated.

Comparing the experimental $i_{Ni,\,max}$ with the calculated $i_{Ni,\,g}$, it can be concluded that, for both nickel concentrations, $i_{Ni,\,max}$ is clearly smaller than $i_{Ni,\,g}$. This means that the limiting current density, determined by diffusion and migration, is not attained for Ni deposition from Ni spare tank solutions.

4.1.2. Effect of Ni^{2+} concentration on the nickel selectivity ratio

The effect of Ni^{2+} concentration on the nickel selectivity ratio was investigated at a constant current density of 100 A m^{-2}. S_{Ni} is plotted against C_{Ni} on a double logarithmic scale in Fig. 3. From Fig. 3, it can be seen that log S_{Ni}

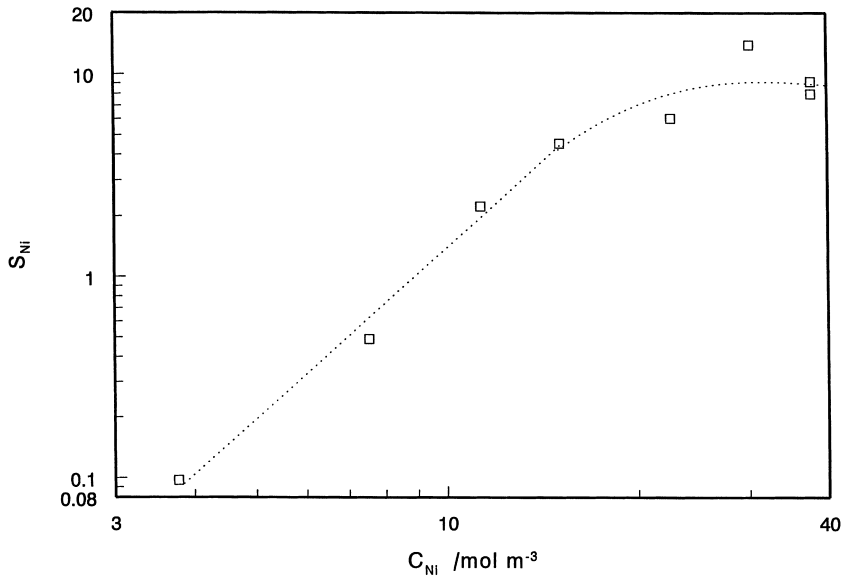

Fig. 3. Nickel selectivity ratio as a function of the nickel ion concentration at a current density of 100 A m^{-2}.

increases linearly with increasing log C_{Ni} up to a maximum of 10 at C_{Ni}=20 mol m^{-3} and thereafter remains constant with increasing Ni concentration.

4.1.3. UV treatment

The effect of UV irradiation on the separate solutions with organic additives was investigated. It was found that UV light irradiation alone, the addition of H_2O_2 or a combination of UV irradiation and addition of H_2O_2 did not break down the organic components of the solutions H(R) and DI. The organic components of the solutions SF/PP(R) and saccharin can be decomposed by UV alone and also in combination with H_2O_2. H_2O_2 alone without UV irradiation has only a negligible effect on the components of the solutions SF/PP(R) and saccharin.

The effect of treating dilute industrial nickel solution containing organic additives by UV was investigated. A fraction of the industrial solution diluted to 5 mM was first irradiated by UV for 1 h, and then the pH was adjusted to 3 by the addition of sulphuric acid solution; thereafter nickel deposition on RDE was carried out. Fig. 4 shows the nickel current density for the treated and untreated solution as a function of the applied current density. From Fig. 4 it follows that there is no effect of the UV treatment of the solution.

4.1.4. Concentration profiles during nickel deposition from a nickel sulphate–boric acid solution

The concentration profiles of selected species in the diffusion layer were calculated for 16 different current densities over a large current density range using a solution containing 40 mol m^{-3} Ni^{2+} and 26 mol m^{-3} H_3BO_3 at pH 6.32, where the partial current densities for Ni deposition and hydrogen evolution are calculated from the results given in Fig. 2. It was found that, at 20 A m^{-2}, the concentrations of $NiOH^+$, $Ni(H_2BO_3)_2$ and $H_2BO_3^-$ increase and the concentrations of H^+ and Ni^{2+} decrease gradually towards the electrode surface. The log $C_j - x$ profiles within the diffusion layer for 360 and 480 A m^{-2} are shown in Figs. 5 and 6. Fig. 5 at 360 A m^{-2} shows clear changes in concentration for the different species. Pronounced changes in the concentration profiles are found at 480 A m^{-2} (Fig. 6). The profiles at 480 A m^{-2} shows a discontinuity at $x=7.8\times10^{-6}$ m. For $x<7.8\times10^{-6}$ m, the Ni^{2+}, $NiOH^+$ and H^+ ion concentrations drop dramatically towards the electrode surface, while the $H_2BO_3^-$ concentration increases sharply. The concentration of $Ni(H_2BO_3)_2$ first increases sharply from $x=10^{-5}$ to 7.8×10^{-6} m and then remains at a constant level towards the electrode surface. The sharp drop in the concentrations of $NiOH^+$ and Ni^{2+} near $x=7.8\times10^{-6}$ m is due to precipitation of $Ni(OH)_2$. It can be concluded that the concentration changes within the diffusion layer are caused by nickel deposition at the electrode surface and by precipitation of $Ni(OH)_2$ at a certain distance from the electrode surface within the diffusion layer.

The effect of the current density on the surface concentrations for $NiOH^+$, H^+, Ni^{2+}, $H_2BO_3^-$ and $Ni(H_2BO_3)_2$ is shown in Fig. 7. Two distinct regions of current density are observable in Fig. 7, namely: (i) the low current density range, $i<300$ A m^{-2}, where the surface concentrations of $NiOH^+$, H^+ and Ni^{2+} decrease slowly while the surface concentrations of $Ni(H_2BO_3^-)_2$ and $H_2BO_3^-$ increase slowly with increasing current density; from the linear log S_{Ni}/log i

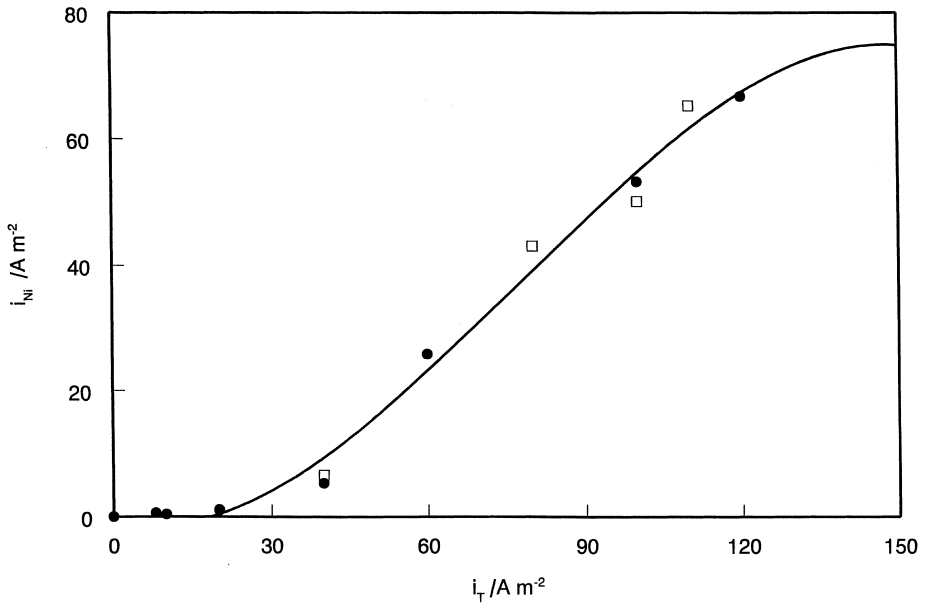

Fig. 4. Effect of UV treatment on the nickel deposition rate for an industrial nickel solution containing 5 mol m^{-3} Ni^{2+} at pH=3 and T=293 K; (●) not UV treated; (□) UV treated.

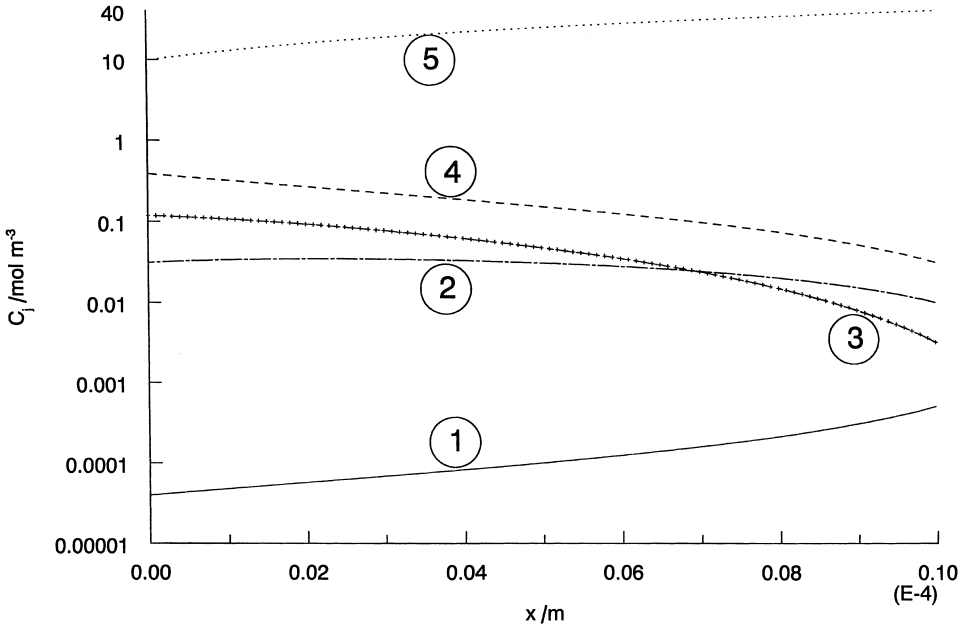

Fig. 5. $\log C_j$ as a function of distance from the surface of the RDE at a current density of 360 A m^{-2}; H^+ (1), $NiOH^+$ (2), $Ni(H_2BO_3)_2$ (3), $H_2BO_3^-$ (4) and Ni^{2+} (5).

relation, it follows that in this area, the kinetics of electrode reactions determine the nickel selectivity ratio S_{Ni} [14]; (ii) the high current density range, i>400 A m^{-2} where the surface concentrations of Ni^{2+} and $NiOH^+$ decrease sharply with increasing current density i_T and become practically zero at 480 A m^{-2}. In this current density range, precipitation of $Ni(OH)_2$ occurs.

4.2. The pilot plant

4.2.1. The nature of deposit

4.2.1.1. Cathode filled with a stack of expanded nickel gauzes. In one experiment, the whole liquid chamber (1 cm thick) was filled with a stack of expanded nickel

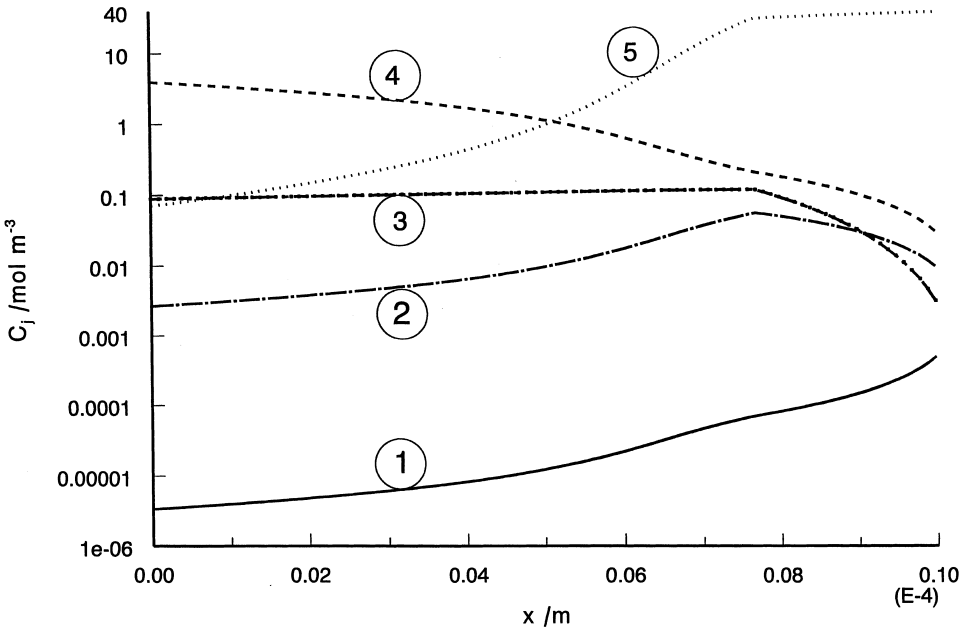

Fig. 6. $\log C_j$ as a function of distance from the surface of the RDE at a current density of 480 A m^{-2}; H^+ (1), $NiOH^+$ (2), $Ni(H_2BO_3)_2$ (3), $H_2BO_3^-$ (4) and Ni^{2+} (5).

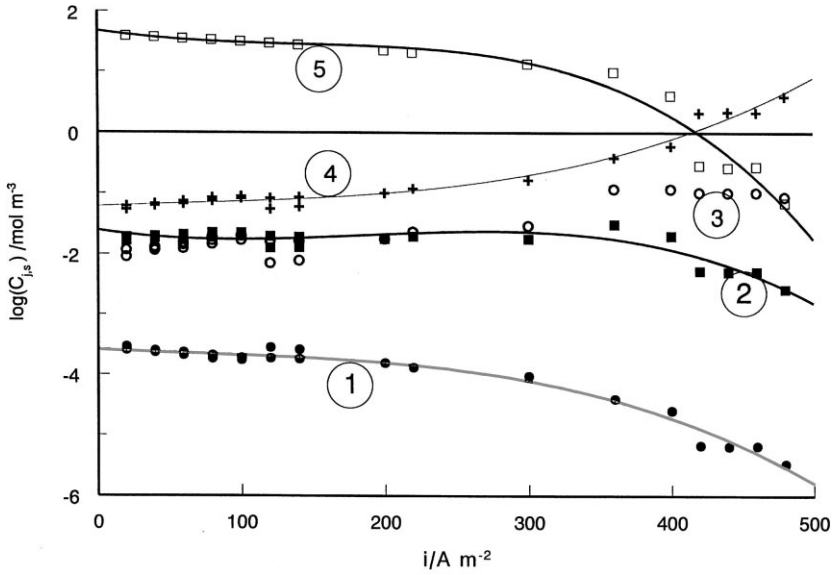

Fig. 7. Log C_j at the surface of the RDE as a function of total current density; H^+ (1), $NiOH^+$ (2), $Ni(H_2BO_3)_2$ (3), $H_2BO_3^-$ (4) and Ni^{2+} (5).

metal gauzes. The cathode was separated from the GDE by a Nafion membrane glued to the GDE. Electrolysis was carried out at 500 A m^{-2}. After 7 days, it was found that nickel was deposited in different forms, such as dendrites, on the expanded gauze closest to the membrane and the growth of the nickel dendrites was directed towards the membrane. These dendrites damaged the membrane and the GDE. To protect the GDE, it was decided to introduce an empty chamber of 1 cm thickness between the GDE and the stack of expanded metal gauzes. Fresh electrolysis was repeated at 250 A m^{-2}. After 2 days, it was found that the whole empty chamber between the GDE membrane and the stack of gauzes was filled with green and black powder. Some metallic nickel was deposited on and close to the membrane. It was found that the membrane was again damaged.

4.2.1.2. Flat plate cathode loaded with low current density. In another experiment, a flat titanium backplate was used as a cathode and the interelectrode gap was 1.5 cm. After an electrolysis at 63 A m^{-2} during 5 days, it was found that a metallic deposit of about 2 mm thick was formed on the flat titanium cathode and dendrite fingers of about 1 cm in length had grown towards the GDE. Analysis of the deposit was carried out using electron probe microanalysis (EPMA) (Superprobe JXA-8600SX Jeol). The results of this analysis showed that the deposit was pure nickel.

4.2.1.3. Flat plate loaded with high current density. With the same construction as in Section 4.2.1.2, the current density was increased to 188 A m^{-2}. After 12 days it was found that the whole liquid compartment was filled with a mixture of green and black powder, and it was also noted that 20% of the Nafion membrane on the GDE was covered with metallic nickel. Analysis of these deposits was performed using EPMA. It was found that the green deposit had high weight contents of oxygen (44%) and nickel (49%). Moreover, other impurities, such as Mg, Si and Ca, were detected in small quantities (in total <5%). Analysis of the black deposit showed that it also contained mainly oxygen (46%) and nickel (53%) and with very small quantities of Mg, Si and Ca.

In [15], it is mentioned that nickel oxyhydroxide is a black precipitate and nickel oxide and nickel hydroxide are greenish precipitates. Moreover, the nickel oxide and nickel hydroxides are non-electron conducting materials. The weight ratio between nickel and oxygen for the black powder is higher than that for the green powder. This supports the conclusion that the black powder is nickel oxyhydroxide and the green powder is a mixture of nickel oxide and hydroxide.

4.2.2. The deposit penetration depth

The deposit penetration depth was investigated for a 5 mm thick stack of three expanded titanium gauzes at 100 and 200 A m^{-2} and using nickel spare tank solutions with nickel concentrations of 5 and 40 mol m^{-3}. The distribution of the deposit on each expanded metal gauze was determined. It was found that, for both current densities, 90% of the deposit was present on the gauze at the GDE side of the stack of expanded titanium gauzes. The middle gauze contained only slightly <10%, while that at the rear side of the stack cathode contained very little deposit.

4.2.3. Electrode configuration

Two different cathode configurations were used, namely a titanium plate and an expanded titanium gauze, to test the effect on nickel deposition. The results are shown in Fig. 8. It can be seen in this figure that, at high geometric current densities calculated on the basis of $4\times20\,cm^2$, the

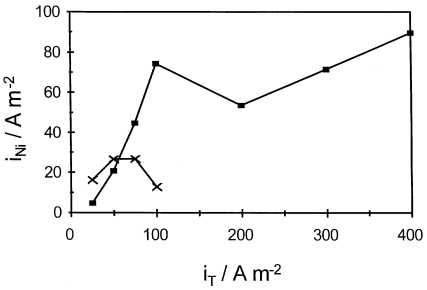

Fig. 8. Nickel deposition current density as a function of total current density for different cathode configurations and for a spare tank solution with 5 mol m^{-3} Ni^{2+} at pH 4 and 293 K; (**X**) flat titanium plate; (■) expanded titanium gauze.

nickel current efficiency for metalic nickel is highest for the expanded titanium gauze electrode. This activity is caused by mass transfer phenomena, as the mass transfer coefficient is larger over an expanded electrode than over a flat surface.

5. Discussion

5.1. Concentrations of species on the electrode surface

The concentration calculations were carried out for a solution containing only $NiSO_4$ and H_3BO_3, whereas the current efficiency measurements were performed with industrial solutions containing $NiCl_2$ and some organic additives in addition to $NiSO_4$ and H_3BO_3.

The concentration of the organic compounds is very small and will not affect significantly the pH of the solution. Moreover, it is likely that the deposition of nickel hydroxide is not affected by the presence of small concentrations of organic compounds.

The industrial solution also contains chloride ions, but their concentration is clearly lower than the sulphate ion concentration. Chloride ions also affect the transport of other ions and, therefore, the concentration profile of each ion within the diffusion layer at the cathode. However, to prevent extensive calculations, a relatively simple composition of the solution has been considered. This means that the conclusions deduced from these model calculations are only useful in a qualitative sense.

From Figs. 5 and 6, it is concluded that an increase in the total current drives the system to an area where precipitation of $Ni(OH)_2$ occurs. The precipitation of $Ni(OH)_2$ occurs at a distance away from the electrode surface and, therefore, the $Ni(OH)_2$ precipitate is not firmly attached to the electrode surface. Due to the depletion of nickel ions on the electrode surface, hydrogen evolution becomes more important, while metal deposition is almost stopped. As Ni^{2+} must cross the precipitation area within the diffusion layer while diffusing towards the electrode surface, most of the Ni^{2+} ions are precipitated out. This phenomenon takes place even at current densities much smaller than the migration–diffusion limiting current density of 959 A m^{-2} for the experiments of Fig. 7, where it is assumed that no nickel hydroxide deposition takes place.

5.2. Form of nickel removal

Nickel deposition from industrial solution has revealed that three types of deposit can be obtained. Which kind of deposit is obtained depends on the electrolysis conditions. As reported, dendrite formation on the Nafion membrane is also a great problem. This implies that the cell design needs to be changed to allow frequent or continuous removal of the deposit in whichever form it may occur. Moreover, the deposits growing on the cathode have to be removed by a scrapes. The use of a three dimensional cathode for nickel deposition gives practically no industrial advantages. After nickel metal deposition occurs on a three-dimensional cathode, this cathode behaves as a planar cathode. A more attractive method would be electrodialysis. In this method, a concentrated nickel solution can be obtained and this solution can be added to the nickel plating bath.

References

[1] E.C.W. Wijnbelt, L.J.J. Janssen, J. Appl. Electrochem. 24 (1994) 1028.
[2] L.J.J. Janssen, The Netherlands Patent 9,101,022 (1991).
[3] I. Portegies Zwart, L.J.J. Janssen, J. Appl. Electrochem. 28 (1998) 1.
[4] H. Dahms, I.M. Croll, J. Electrochem. Soc. 112 (1965) 771.
[5] D. Gangasingh, J.B. Talbot, J. Electrochem. Soc. 138 (1991) 3605.
[6] S. Hessami, C.W. Tobias, J. Electrochem. Soc. 136 (1989) 3611.
[7] W.C. Grande, J.B. Talbot, J. Electrochem. Soc. 140 (1993) 675.
[8] W.C. Grande, J.B. Talbot, Proc. Electrochem. Soc. 90 (1991) 437.
[9] B.V. Tilak, A.S. Gendron, M.A. Mosoiu, J. Appl. Electrochem. 7 (1977) 495.
[10] J.S. Newman, Electrochemical Systems, 1st Edition, Prentice-Hall, Englewood Cliffs, NJ, 1973, p. 230.
[11] J.K. Park, K.J. Lee, J. Chem. Eng. Data 39 (1994) 891.
[12] R.M.Smith, A.E. Martell, Critical Stability Constants, Plenum Press, New York, 1989.
[13] B.W. Rossiter, J.F. Hamilton, Physical Methods of Chemistry, Wiley, New York, 1986.
[14] Y.P. Perelygin, Russ. J. Electrochem. 30 (1994) 10.
[15] D.J. Ives, G.J. Janz, Reference Electrodes: Theory and Practice, Academic Press, New York, 1961, p. 332.